Journal of the Physical Society of Japan
Vol. 71, No. 11, November, 2002, pp. 2753–2760

Presence of Perfectly Conducting Channel in Metallic Carbon Nanotubes

Tsuneya ANDO and Hidekatsu SUZUURA

Department of Physics, Tokyo Institute of Technology, 2-12-1 Ookayama, Meguro-ku, Tokyo 152-8551

(Received July 24, 2002)

It is proved that a conducting channel transmitting perfectly without backscattering is present independent of energy in metallic carbon nanotubes for scatterers with potential range larger than the lattice constant. In the case that several traveling channels are present, the conductance decreases from the ideal value determined by the number of traveling modes to the single-channel value when the length exceeds the mean free path determined by a Boltzmann transport equation. Further, inelastic scattering makes the conductance decrease in proportion to the inverse of the length in qualitative agreement with the Boltzmann result.

KEYWORDS: graphite, carbon nanotube, impurity scattering, conductance quantization, effective-mass theory
DOI: 10.1143/JPSJ.71.2753

1. Introduction

Carbon nanotubes (CN's) are quasi-one-dimensional materials made of sp^2-hybridized carbon networks[1] and have been a subject of an extensive study. In particular, the electronic structure of a single CN has been studied theoretically, which predicted that CN becomes either metallic or semiconducting depending on its chiral vector, i.e., boundary conditions in the circumference direction.[2–11] These predictions have been confirmed by Raman experiments[12] and direct measurements of local density of states by scanning tunneling spectroscopy.[13–15] In this paper we shall investigate effects of potential scattering in metallic nanotubes in the case of the presence of several current carrying channels.

Transport properties are particularly interesting because of their unique topological structures.[16] For impurity scattering, it was shown theoretically that there is no backscattering for potentials with a range larger than the lattice constant in metallic CN's.[17] The absence of backscattering was related to Berry's phase acquired by a rotation in the wave-vector space in the system described by a $\boldsymbol{k}\cdot\boldsymbol{p}$ Hamiltonian.[18] It has been confirmed by numerical calculations in a tight-binding model.[19] There have been some reports on experiments which support this theoretical prediction.[20,21]

In understanding transport properties of nanotubes, a $\boldsymbol{k}\cdot\boldsymbol{p}$ method or an effective-mass approximation[11] has been quite useful. It has been used successfully in the study of wide varieties of electronic properties of CN's. Some of such examples are magnetic properties[22] including the Aharonov–Bohm effect on the band gap, optical absorption spectra,[23] exciton effects,[24] lattice instabilities in the absence[25,26] and presence of a magnetic field,[27] magnetic properties of ensembles of nanotubes,[28] effects of spin-orbit interaction,[29] and electronic properties of nanotube caps.[30]

Effects of scattering by a lattice vacancy in armchair nanotubes have been studied within a tight-binding model.[31,32] It has been shown that the conductance at zero energy in the absence of a magnetic field is quantized into zero, one, or two times of the conductance quantum $e^2/\pi\hbar$ for $\Delta N_{\rm AB} \geq 2$, $\Delta N_{\rm AB} = 1$, and $\Delta N_{\rm AB} = 0$, respectively, where $\Delta N_{\rm AB}$ is the difference between the number of removed atoms at A and B sites.[32,33] This rule was analytically derived in a $\boldsymbol{k}\cdot\boldsymbol{p}$ scheme.[34,35] Calculations for realistic defects were performed also.[36] Long wavelength phonons and electron–phonon scattering have been studied.[37]

In this paper, we consider scattering in metallic carbon nanotubes containing scatterers with potential range larger than or comparable to the lattice constant in the case that several traveling modes are present at the Fermi energy. We shall prove analytically the presence of a channel transmitted through the system without backscattering. Further, numerical calculations are performed to clarify how the conductance decreases from the ideal value determined by the number of traveling modes to that of a single mode with the increase of the length. Effects of inelastic scattering are studied also within a model that an electron looses its phase memory after traveling over a distance determined by a phase coherence length.

The paper is organized as follows: In §2 the treatment of electronic states in a $\boldsymbol{k}\cdot\boldsymbol{p}$ scheme is reviewed briefly. Some exact properties of reflection coefficients in metallic nanotubes are derived in §3. Numerical results on the length dependence of the conductance are presented in §4. In §5, a Boltzmann transport equation is shown to give a finite conductivity when there are several current carrying bands at the Fermi level, quite in contrast to the exact result showing the presence of a perfectly transmitting channel. In §6 a model calculation is performed to clarify effects of inelastic scattering.

2. Effective-Mass Equation

The lattice structure of a two-dimensional (2D) graphite and corresponding first Brillouin zone are shown in Fig. 1. A unit cell contains two carbon atoms denoted by A and B. The coordinate system (x', y') is fixed onto the graphite sheet (x' is in the direction of $\boldsymbol{a}$ with $a = |\boldsymbol{a}|$ being the lattice constant) and (x, y) is chosen in such a way that the x axis is in the chiral direction of CN, i.e., the direction along the circumference, and the y axis in the direction of the axis. The angle between the x and x' direction is called a chiral angle and denoted as η. We have $\eta = 0$ for a zig-zag nanotube and $\eta = \pi/6$ for an armchair nanotube. The conduction and valence bands of 2D graphite cross each other at K and K′ points where the bands have approximately a linear dispersion as a function of the wave vector.

In the effective-mass approximation, the electronic states

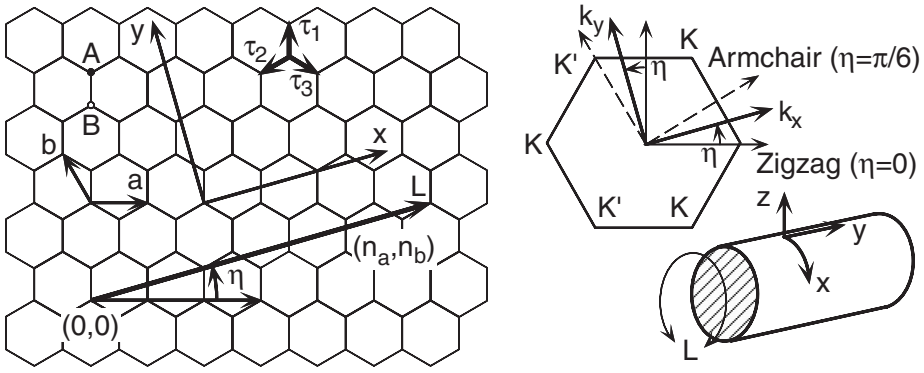

Fig. 1. (a) Lattice structure of two-dimensional graphite sheet. η is the chiral angle. The coordinates are chosen in such a way that x is along the circumference of a nanotube and y is along the axis. (b) The first Brillouin zone and K and K′ points. (c) The coordinates for a nanotube.

of a 2D graphite near a K point are described by a $\boldsymbol{k}\cdot\boldsymbol{p}$ equation as[11,38]

$$\gamma(\boldsymbol{\sigma}\cdot\hat{\boldsymbol{k}})\boldsymbol{F}(\boldsymbol{r}) = \varepsilon\boldsymbol{F}(\boldsymbol{r}), \tag{2.1}$$

or

$$\gamma\begin{pmatrix} 0 & \hat{k}_x - \mathrm{i}\hat{k}_y \\ \hat{k}_x + \mathrm{i}\hat{k}_y & 0 \end{pmatrix}\begin{pmatrix} F_{\mathrm{A}}(\boldsymbol{r}) \\ F_{\mathrm{B}}(\boldsymbol{r}) \end{pmatrix} = \varepsilon\begin{pmatrix} F_{\mathrm{A}}(\boldsymbol{r}) \\ F_{\mathrm{B}}(\boldsymbol{r}) \end{pmatrix}, \tag{2.2}$$

where γ is the band parameter, $\boldsymbol{\sigma} = (\sigma_x, \sigma_y)$ is the Pauli spin matrix, $\hat{\boldsymbol{k}} = (\hat{k}_x, \hat{k}_y)$ is a wave vector operator defined by $\hat{\boldsymbol{k}} = -\mathrm{i}\nabla$, and F_{A} and F_{B} represent the amplitude at A and B carbon atoms, respectively. The wave functions and energies of this Hamiltonian are written as

$$\boldsymbol{F}_{s\boldsymbol{k}}(\boldsymbol{r}) = \frac{1}{\sqrt{LA}}\exp(\mathrm{i}\boldsymbol{k}\cdot\boldsymbol{r})\boldsymbol{F}_{s\boldsymbol{k}}, \tag{2.3}$$

$$\varepsilon_s(\boldsymbol{k}) = s\gamma|\boldsymbol{k}|, \tag{2.4}$$

where L is the circumference of CN, A is the length, and $s = +1$ and -1 denote conduction and valence bands, respectively. In metallic CN's the wave vector in the k_x direction is quantized into $k_x = \kappa(n)$ with $\kappa(n) = 2\pi n/L$ where n is an integer. In general, we can write eigenvector $\boldsymbol{F}_{s\boldsymbol{k}}$ as

$$\boldsymbol{F}_{s\boldsymbol{k}} = \exp[\mathrm{i}\phi_s(\boldsymbol{k})]R^{-1}[\theta(\boldsymbol{k})]|s), \tag{2.5}$$

where $\phi_s(\boldsymbol{k})$ is an arbitrary phase factor, $\theta(\boldsymbol{k})$ is the angle between wave vector $\boldsymbol{k}$ and the k_y axis, i.e., $k_x + \mathrm{i}k_y = \mathrm{i}|\boldsymbol{k}|\mathrm{e}^{\mathrm{i}\theta(\boldsymbol{k})}$, $R(\theta)$ is a spin-rotation operator, given by

$$R(\theta) = \exp\left(\mathrm{i}\frac{\theta}{2}\sigma_z\right) = \begin{pmatrix} \exp(+\mathrm{i}\theta/2) & 0 \\ 0 & \exp(-\mathrm{i}\theta/2) \end{pmatrix}, \tag{2.6}$$

with σ_z being a Pauli matrix, and $|s)$ is the eigenvector for the state with $\boldsymbol{k}$ in the positive k_y direction, given by

$$|s) = \frac{1}{\sqrt{2}}\begin{pmatrix} -\mathrm{i}s \\ 1 \end{pmatrix}. \tag{2.7}$$

Obviously, we have

$$R(\theta_1)R(\theta_2) = R(\theta_1 + \theta_2), \quad R(-\theta) = R^{-1}(\theta), \quad \text{etc.} \tag{2.8}$$

Further, because $R(\theta)$ describes the rotation of a spin, it has the property

$$R(\theta \pm 2\pi) = -R(\theta), \tag{2.9}$$

which gives $R(-\pi) = -R(+\pi)$. In order to define states and corresponding wave functions uniquely, we shall assume in the following that

$$-\pi < \theta(\boldsymbol{k}) \le +\pi. \tag{2.10}$$

By choosing the phase $\phi_s(\boldsymbol{k})$ in an appropriate manner, the wave function can be chosen as either continuous or discontinuous across the point corresponding to $\theta = +\pi$ and $-\pi$ in the $\boldsymbol{k}$ space. The results are certainly independent of such choices.

3. Reflection Coefficient

In the following, we shall consider the reflection coefficient $r_{\bar{\beta}\alpha}$ from a state with wave vector $\boldsymbol{k}_\alpha$ to a state with $\boldsymbol{k}_{\bar{\beta}} \equiv -\boldsymbol{k}_\beta$ due to an arbitrary external potential having a range larger than or comparable to the lattice constant in a 2D graphite sheet. Here, $\bar{\beta}$ stands for the state with wave vector opposite to β. Only difference arising in nanotubes is discretization of the wave vector in the k_x direction as mentioned above. We shall confine ourselves to states in the vicinity of the K point, but the extension to states near a K′ point is straightforward.

Introduce a T matrix defined by

$$T = V + V\frac{1}{\varepsilon - \mathcal{H}_0}V + V\frac{1}{\varepsilon - \mathcal{H}_0}V\frac{1}{\varepsilon - \mathcal{H}_0}V + \cdots, \tag{3.1}$$

where V is the impurity potential given by a diagonal matrix, i.e.,

$$V = V(\boldsymbol{r})\begin{pmatrix} 1 & 0 \\ 0 & 1 \end{pmatrix}, \tag{3.2}$$

ε is the energy, and $\mathcal{H}_0 = \gamma\boldsymbol{\sigma}\cdot\boldsymbol{k}$ is the Hamiltonian in the absence of the potential. The $(p+1)$th order term of the T matrix corresponding to scattering $\alpha \to \bar{\beta}$ is written as

$$
\begin{aligned}
(s,\bar{\boldsymbol{\beta}}|T^{(p+1)}|s,\alpha) = {} & \frac{1}{LA}\sum_{s_1\boldsymbol{k}_1}\frac{1}{LA}\sum_{s_2\boldsymbol{k}_2}\cdots\frac{1}{LA}\sum_{s_p\boldsymbol{k}_p} \\
& \times \frac{V(\boldsymbol{k}_{\bar{\beta}}-\boldsymbol{k}_p)\cdots V(\boldsymbol{k}_2-\boldsymbol{k}_1)V(\boldsymbol{k}_1-\boldsymbol{k}_\alpha)}{[\varepsilon-\varepsilon_{s_p}(\boldsymbol{k}_p)]\cdots[\varepsilon-\varepsilon_{s_2}(\boldsymbol{k}_2)][\varepsilon-\varepsilon_{s_1}(\boldsymbol{k}_1)]} \\
& \times \mathrm{e}^{-\mathrm{i}\phi_s(\boldsymbol{k}_{\bar{\beta}})}(s|R[\theta(\boldsymbol{k}_{\bar{\beta}})]R^{-1}[\theta(\boldsymbol{k}_p)]|s_p) \\
& \times\cdots\times(s_2|R[\theta(\boldsymbol{k}_2)]R^{-1}[\theta(\boldsymbol{k}_1)]|s_1) \\
& \times(s_1|R[\theta(\boldsymbol{k}_1)]R^{-1}[\theta(\boldsymbol{k}_\alpha)]|s)\mathrm{e}^{\mathrm{i}\phi_s(\boldsymbol{k}_\alpha)},
\end{aligned}
\tag{3.3}
$$

where $V(\boldsymbol{k})$ is a Fourier transform of the impurity potential and phase factors $\exp[\mathrm{i}\phi_{s_j}(\boldsymbol{k}_j)]$ have been canceled out for all the intermediate states $j=1,\ldots,p$.

For each term in eq. (3.3), there is a term obtained through the replacement

$$
(s_1,\boldsymbol{k}_1)\to(s_p,\boldsymbol{k}_{\bar{p}}),\quad (s_2,\boldsymbol{k}_2)\to(s_{p-1},\boldsymbol{k}_{\overline{p-1}}),\quad \text{etc.},
\tag{3.4}
$$

where $\boldsymbol{k}_{\bar{p}}=-\boldsymbol{k}_p$. Both matrix elements of the impurity potential and energy denominators are same as those for the corresponding quantities of $(s,\bar{\boldsymbol{\alpha}}|T^{(p+1)}|s,\beta)$. Figure 2 shows a schematic illustration of processes $(s,\bar{\boldsymbol{\beta}}|T^{(p+1)}|s,\alpha)$ and $(s,\bar{\boldsymbol{\alpha}}|T^{(p+1)}|s,\beta)$.

Define

$$
\begin{aligned}
S^{(p+1)}_{\bar{\beta}\alpha} = {} & (s|R[\theta(\boldsymbol{k}_{\bar{\beta}})]R^{-1}[\theta(\boldsymbol{k}_p)]|s_p) \\
& \times\cdots\times(s_2|R[\theta(\boldsymbol{k}_2)]R^{-1}[\theta(\boldsymbol{k}_1)]|s_1) \\
& \times(s_1|R[\theta(\boldsymbol{k}_1)]R^{-1}[\theta(\boldsymbol{k}_\alpha)]|s).
\end{aligned}
\tag{3.5}
$$

This quantity describes matrix elements of a rotation in the spin space corresponding to $(s,\bar{\boldsymbol{\beta}}|T^{(p+1)}|s,\alpha)$. Under the replacement (3.4), it changes into $S^{(p+1)\prime}_{\bar{\beta}\alpha}$ with

$$
\begin{aligned}
S^{(p+1)\prime}_{\bar{\beta}\alpha} = {} & (s|R[\theta(\boldsymbol{k}_{\bar{\beta}})]R^{-1}[\theta(\boldsymbol{k}_{\bar{1}})]|s_1) \\
& \times\cdots\times(s_{p-1}|R[\theta(\boldsymbol{k}_{\overline{p-1}})]R^{-1}[\theta(\boldsymbol{k}_{\bar{p}})]|s_p) \\
& \times(s_p|R[\theta(\boldsymbol{k}_{\bar{p}})]R^{-1}[\theta(\boldsymbol{k}_\alpha)]|s).
\end{aligned}
\tag{3.6}
$$

According to the present definition of the angle given by eq. (2.10), we have

$$
\theta(-\boldsymbol{k})=\theta(\boldsymbol{k})+\pi\,\mathrm{sgn}[-\theta(\boldsymbol{k})],
\tag{3.7}
$$

where $\mathrm{sgn}(t)$ is the signature of t defined by

$$
\mathrm{sgn}(t)=\begin{cases}+1 & (t>0),\\ +1 & (t=0),\\ -1 & (t<0).\end{cases}
\tag{3.8}
$$

Note the definition for $t=0$. Note also that the choice $\theta(-\boldsymbol{k}_j)=\theta(\boldsymbol{k}_j)-\pi$ or $\theta(-\boldsymbol{k}_j)=\theta(\boldsymbol{k}_j)+\pi$ causes only the difference in the signature of the wave function. For intermediate states, therefore, the results are independent of these choices because $\theta(-\boldsymbol{k}_j)$ always appears in a pair, In the following we shall put $\theta(-\boldsymbol{k}_j)=\theta(\boldsymbol{k}_j)-\pi$ for $j=1,\ldots,p$ and have

$$
\begin{aligned}
(s|R[\theta(\boldsymbol{k}_{\bar{\beta}})]R^{-1}[\theta(\boldsymbol{k}_{\bar{1}})]|s_1) &= (s_1|R[\theta(\boldsymbol{k}_1)]R^{-1}[\theta(\boldsymbol{k}_{\bar{\beta}})+\pi]|s)^*, \\
&\cdots \\
(s_{p-1}|R[\theta(\boldsymbol{k}_{\overline{p-1}})]R^{-1}[\theta(\boldsymbol{k}_{\bar{p}})]|s_p) &= (s_p|R[\theta(\boldsymbol{k}_p)]R^{-1}[\theta(\boldsymbol{k}_{p-1})]|s_{p-1})^*, \\
(s_p|R[\theta(\boldsymbol{k}_{\bar{p}})]R^{-1}[\theta(\boldsymbol{k}_\alpha)]|s) &= (s|R[\theta(\boldsymbol{k}_\alpha)+\pi]R^{-1}[\theta(\boldsymbol{k}_p)]|s_p)^*.
\end{aligned}
\tag{3.9}
$$

Now, with the use of eq. (3.7) we have

$$
\begin{aligned}
R^{-1}[\theta(\boldsymbol{k}_{\bar{\beta}})+\pi] &= -\,\mathrm{sgn}[-\theta(\boldsymbol{k}_\beta)]R^{-1}[\theta(\boldsymbol{k}_\beta)], \\
R[\theta(\boldsymbol{k}_\alpha)+\pi] &= +\,\mathrm{sgn}[-\theta(\boldsymbol{k}_\alpha)]R[\theta(\boldsymbol{k}_{\bar{\alpha}})].
\end{aligned}
\tag{3.10}
$$

Therefore, we have

$$
S^{(p+1)\prime}_{\bar{\beta}\alpha} = -\,\mathrm{sgn}[-\theta(\boldsymbol{k}_\alpha)]\,\mathrm{sgn}[-\theta(\boldsymbol{k}_\beta)]S^{(p+1)*}_{\bar{\alpha}\beta},
\tag{3.11}
$$

where $S^{p+1}_{\bar{\alpha}\beta}$ is obtained from eq. (3.5) just by the exchange

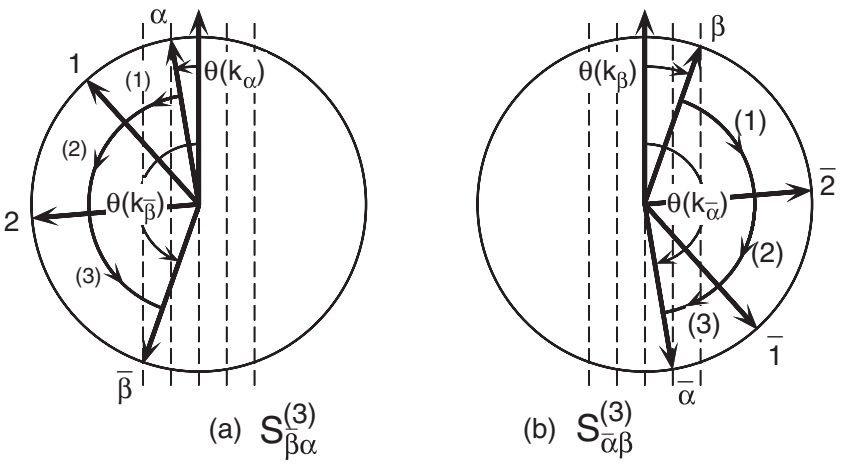

Fig. 2. A scattering process and its time reversal process. The circles represent the Fermi surface in two-dimensional graphite and the dashed lines quantized wave vectors in nanotubes. $S_{\bar{\beta}\alpha}$ represents scattering $\alpha\to\bar{\boldsymbol{\beta}}$ and $S_{\bar{\alpha}\beta}$ $\beta\to\bar{\boldsymbol{\alpha}}$, where $\bar{\boldsymbol{\alpha}}$ and $\bar{\boldsymbol{\beta}}$ represent time reversal states of α and β, respectively.

$\alpha \leftrightarrow \beta$.

More explicitly, we have

$$(s|R(\theta)R^{-1}(\theta')|s') = \begin{cases} \cos[(\theta-\theta')/2] & (s=s'), \\ -\mathrm{i}\sin[(\theta-\theta')/2] & (s\neq s'), \end{cases} \tag{3.12}$$

which is either real or pure imaginary. Because the number of matrix elements for different bands is always even in the expression of $S^{(p+1)}$, we see immediately that $S^{(p+1)}$ is given by a real number. Therefore, we have

$$S^{(p+1)\prime}_{\bar{\beta}\alpha} = -\operatorname{sgn}[-\theta(\boldsymbol{k}_\alpha)]S^{(p+1)}_{\bar{\alpha}\beta}\operatorname{sgn}[-\theta(\boldsymbol{k}_\beta)]. \tag{3.13}$$

This immediately gives the relation

$$T_{\bar{\beta}\alpha} = -u_\alpha T_{\bar{\alpha}\beta}u^*_\beta, \tag{3.14}$$

with

$$T_{\bar{\beta}\alpha} \equiv (s,\bar{\beta}|T|s,\alpha), \tag{3.15}$$

and

$$u_\alpha = \operatorname{sgn}[-\theta(\boldsymbol{k}_\alpha)]\mathrm{e}^{\mathrm{i}\phi_s(\boldsymbol{k}_\alpha)+\mathrm{i}\phi_s(\boldsymbol{k}_{\bar{\alpha}})}, \tag{3.16}$$

which satisfies $|u_\alpha| = 1$.

The above relation for the T matrix immediately gives

$$r_{\bar{\beta}\alpha} = -u_\alpha r_{\bar{\alpha}\beta}u^*_\beta. \tag{3.17}$$

This leads to the absence of backward scattering

$$r_{\bar{\alpha}\alpha} = -r_{\bar{\alpha}\alpha} = 0, \tag{3.18}$$

shown previously.[17,18] Define the reflection matrix r by

$$[r]_{\alpha\beta} = r_{\bar{\alpha}\beta}, \tag{3.19}$$

and a unitary matrix U by

$$U_{\alpha\beta} = u_\alpha\delta_{\alpha\beta}. \tag{3.20}$$

Then, we have

$$r = -U\,{}^t r U^\dagger, \tag{3.21}$$

where ${}^t r$ is the transpose of r.

In general we have $\det {}^tP = \det P$ for any matrix P. In metallic nanotubes, the number of traveling modes n_c is always given by an odd integer and therefore $\det(-r) = -\det(r)$, leading to

$$\det(r) = 0. \tag{3.22}$$

By definition, $r_{\bar{\beta}\alpha}$ represents the amplitude of an out-going mode $\bar{\beta}$ with wave function $\psi_{\bar{\beta}}(\boldsymbol{r})$ for the reflected wave corresponding to an in-coming mode α with wave function $\psi_\alpha(\boldsymbol{r})$, i.e.,

$$\Psi_\alpha(\boldsymbol{r}) = \psi_\alpha(\boldsymbol{r}) + \sum_{\beta=1}^{n_\mathrm{c}} \psi_{\bar{\beta}}(\boldsymbol{r})r_{\bar{\beta}\alpha}, \tag{3.23}$$

where $\Psi_\alpha(\boldsymbol{r})$ is the wave function in the left hand side corresponding to mode α. The vanishing determinant of r, i.e., eq. (3.22), shows that there exists at least one nontrivial solution for the equation

$$\sum_{\alpha=1}^{n_\mathrm{c}} r_{\bar{\beta}\alpha}a_\alpha = 0. \tag{3.24}$$

Then, there is no reflected wave for the incident wave function $\sum_\alpha a_\alpha\psi_\alpha(\boldsymbol{r})$. As a matter of fact, eq. (3.23) gives

$$\Psi(\boldsymbol{r}) = \sum_{\alpha=1}^{n} a_\alpha\Psi_\alpha(\boldsymbol{r}) = \sum_{\alpha=1}^{n} a_\alpha\psi_\alpha(\boldsymbol{r}), \tag{3.25}$$

demonstrating the presence of a mode which is transmitted through the system with probability one without being scattered back.

This conclusion is a natural extension of the absence of backward scattering when the Fermi level lies in the range corresponding to the presence of a single traveling channel proven previously.[17,18] It is interesting to note that a perfect channel can exist when the number n_c of the traveling channels is odd and cannot when n_c is an even integer because $\det(r) \neq 0$ in this case. In fact, in a quantum wire with a strong spin-orbit interaction similar symmetry relations between reflection coefficients exist but the mode number is always even.[39]

The relation given by eq. (3.17) can be derived also by the property of a time reversal operator. Corresponding to the 2×2 equation containing Pauli's spin matrices, a time reversal operation T is defined as

$$\psi^T = K\psi^*, \tag{3.26}$$

where the wave function is denoted by ψ for convenience, ψ^* represents the complex conjugate of ψ, and K is an antisymmetric unitary matrix

$$K = -\mathrm{i}\sigma_y = \begin{pmatrix} 0 & -1 \\ 1 & 0 \end{pmatrix}. \tag{3.27}$$

The corresponding operation for an operator P is given by

$$P^T = K\,{}^t P K^{-1}. \tag{3.28}$$

Note that

$$K^2 = -1. \tag{3.29}$$

For this definition, we have the identity

$$(\psi_1, P\psi_2) = (\psi_2^T, P^T\psi_1^T), \tag{3.30}$$

where (ψ,ψ') stands for the inner product of ψ and ψ'.

It is easy to show that the Hamiltonian $\mathcal{H}_0$ in the absence of scatterers is invariant under the time reversal operation. Further, the potential is given by a real and diagonal matrix and therefore invariant also. Consequently the T matrix is also invariant under time reversal. Under the time reversal operation, the wave functions are transformed as

$$\begin{aligned} \psi^T_{s\alpha} &= -s\,u^*_\alpha\psi_{s\bar{\alpha}}, \\ \psi^T_{s\bar{\alpha}} &= s\,u^*_\alpha\psi_{s\alpha}, \end{aligned} \tag{3.31}$$

which show that $\psi_{s\alpha}$ and $\psi_{s\bar{\alpha}}$ are indeed connected to each other through the time reversal. With the use of eq. (3.31), we have

$$(\psi^T_{s\alpha})^T = -s\,u_\alpha\psi^T_{s\bar{\alpha}} = -\psi_{s\alpha}, \tag{3.32}$$

which agrees with the result obtained directly using eq. (3.29),

$$(\psi^T_{s\alpha})^T = K^2\psi_{s\alpha} = -\psi_{s\alpha}. \tag{3.33}$$

Because of the time-reversal invariance of T matrix, we have

$$T_{\beta\alpha} = (\psi_\beta, T\psi_\alpha) = (\psi_\alpha^T, T\psi_\beta^T), \tag{3.34}$$

which gives the relation

$$T_{\beta\alpha} = u_\alpha T_{\bar{\alpha}\bar{\beta}} u_\beta^*, \tag{3.35}$$

showing that transmission coefficient $t_{\beta\alpha}$ is same as that of the time reversal processes $t_{\bar{\alpha}\bar{\beta}}$ apart from a trivial phase factor arising from the phase of the wave functions, i.e., $t_{\beta\alpha} = u_\alpha t_{\bar{\alpha}\bar{\beta}} u_\beta^*$ and $|t_{\beta\alpha}|^2 = |t_{\bar{\alpha}\bar{\beta}}|^2$.

For reflection processes, on the other hand, we have

$$T_{\bar{\beta}\alpha} = (\psi_{\bar{\beta}}, T\psi_\alpha) = (\psi_\alpha^T, T\psi_{\bar{\beta}}^T), \tag{3.36}$$

which gives

$$T_{\bar{\beta}\alpha} = -u_\alpha T_{\bar{\alpha}\beta} u_\beta^*. \tag{3.37}$$

This is equivalent to eq. (3.17) or eq. (3.21). The negative sign in the right hand side appears because apart from a trivial phase factor ψ_α^T can be replaced by $\psi_{\bar{\alpha}}$ while $\psi_{\bar{\beta}}^T$ should be replaced by $-\psi_\beta$. The time reversal symmetry does not give any relation between the reflection coefficients for waves incident from left and those from right.

Because the phase of the wave function can be chosen arbitrarily as long as it is uniquely defined for each state, it is possible to choose phases in such a way that the transmission coefficients satisfy $t_{\bar{\alpha}\bar{\beta}} = -t_{\beta\alpha}$ and $r_{\bar{\alpha}\beta} = r_{\bar{\beta}\alpha}$ for some α and β. However, it is impossible to choose phases so as to make all transmission coefficients antisymmetric and reflection coefficients symmetric. In fact, the symmetry for diagonal terms is independent of phases, i.e., $t_{\alpha\alpha} = t_{\bar{\alpha}\bar{\alpha}}$ and $r_{\bar{\alpha}\alpha} = -r_{\bar{\alpha}\alpha}$. Note, further, that the determinant of the reflection matrix vanishes independent of such different choices of the phase.

4. Numerical Results

In order to see the dependence of the conductance on the length of CN explicitly, we shall consider a model system described by scatterers with potential

$$V(\boldsymbol{r}) = \sum_i u_i \delta(\boldsymbol{r} - \boldsymbol{r}_i), \tag{4.1}$$

where $\boldsymbol{r}_i$ denotes the position of the ith scatterer and u_i its strength. In actual calculations, $\boldsymbol{r}_i$ distributes randomly and equal amount of attractive and repulsive scatterers are assumed, i.e., $u_i = \pm u$. In the lowest Born approximation the scattering strength is characterized by the dimensionless quantity

$$W = \frac{n_{\mathrm{i}} \langle |u_i|^2 \rangle}{4\pi\gamma^2} = \frac{n_{\mathrm{i}} u^2}{4\pi\gamma^2}, \tag{4.2}$$

where n_{i} is the concentration of impurities in a unit area and $\langle \cdots \rangle$ means the average over scatterers.[40]

It is straightforward to calculate a scattering matrix for an impurity given by eq. (4.1) and a conductance of a finite-length nanotube containing many impurities, combining scattering matrices as discussed previously.[17,41] Figure 3 shows some examples of the length dependence of the calculated conductance for long-range scatterers for different values of the energy. There are three and five traveling modes for $1 < \varepsilon L/2\pi\gamma < 2$ and $2 < \varepsilon L/2\pi\gamma < 3$, respectively. The arrows show the mean free path of traveling modes obtained by solving the Boltzmann transport equation (see the next section). We have chosen $W^{-1} = 1000$ in Fig. 3(a) and $W^{-1} = 100$ in (b). Although detailed behavior varies as a function of energy relative to the band edge and of W, we can safely conclude that the relevant length scale over which the conductance decreases down to the single-channel result is given by the mean free path.

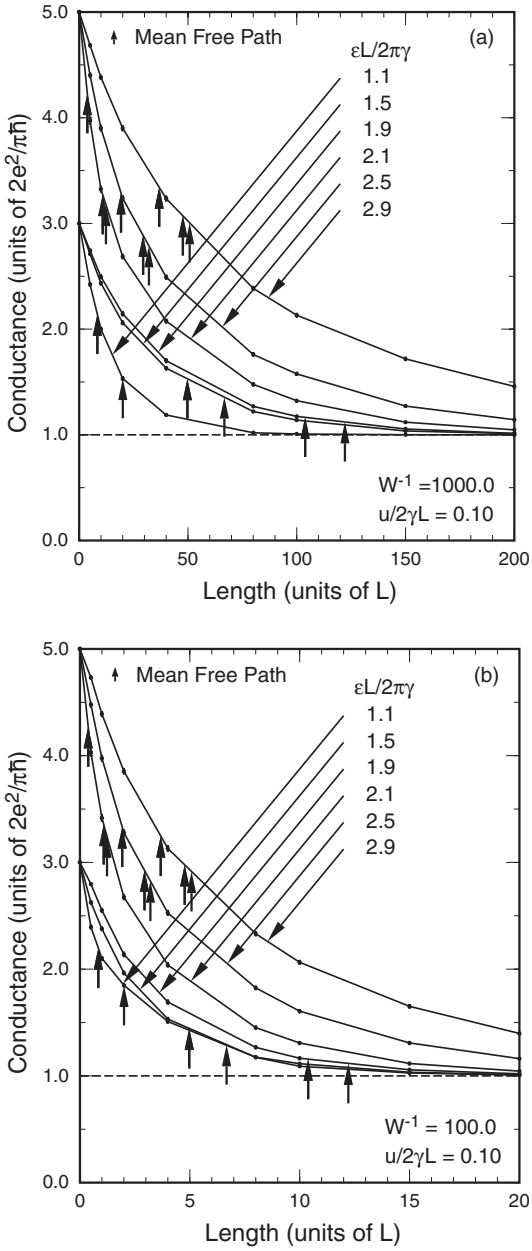

Fig. 3. An example of the length dependence of the calculated conductance for (a) $W^{-1} = 1000$ and (b) $W^{-1} = 100$. The arrows show the mean free path of traveling modes obtained by solving the Boltzmann transport equation. For lower three curves there are three bands with $n = 0$ and ± 1 and for upper three curves there are five bands with $n = 0$, ± 1, and ± 2. The mean free path is same for bands with same $|n|$ and decreases with the increase of $|n|$.

5. Transport Equation

The transport equation in a CN is the same as that in quantum wires[42] and written as

$$-\frac{e}{\hbar}E\frac{\partial g_{mk}}{\partial k}=\sum_{m'k'}W_{m'k'mk}(g_{m'k'}-g_{mk}), \tag{5.1}$$

where E is the electric field in the y direction and g_{mk} is the distribution function for states specified by the wave vector k in the y direction and the band index m. The scattering probability is given in the Born approximation by

$$W_{m'k'mk}=\frac{2\pi}{\hbar}\langle|V_{m'k'mk}|^2\rangle\delta(\varepsilon_{m'k'}-\varepsilon_{mk}), \tag{5.2}$$

where $V_{m'k'mk}$ is the scattering amplitude.

The transport equation can be solved to the lowest order in the electric field as

$$g_{mk}=f(\varepsilon_{mk})+eEv_{mk}\tau_{mk}\frac{\partial f}{\partial\varepsilon}(\varepsilon_{mk}), \tag{5.3}$$

where $f(\varepsilon)$ is the Fermi distribution function, τ_{mk} is the relaxation time, and v_{mk} is the group velocity. Substituting eq. (5.3) into eq. (5.1), we obtain the following equation for the mean free path $\Lambda_m(\varepsilon)=|v_{mk}|\tau_m$ for band m:

$$\sum_{m'}(K_{m-m'+}-K_{m+m'+})\Lambda_{m'}(\varepsilon)=1, \tag{5.4}$$

where m and m' denote the bands crossing the energy ε, and $+$ $(-)$ the wave vector corresponding to the positive (negative) velocity in the y direction. The kernel for the transport equation is given by

$$K_{\nu\mu}=\frac{A\langle|V_{\nu\mu}|^2\rangle}{\hbar^2|v_\mu v_\nu|}, \tag{5.5}$$

for $\nu\neq\mu$, where v_μ is the velocity of mode $\mu\equiv(m\pm)$. The diagonal elements are defined by

$$K_{\mu\mu}=-\sum_{\nu\neq\mu}K_{\nu\mu}. \tag{5.6}$$

The conductivity becomes

$$\sigma=\int d\varepsilon\left(-\frac{\partial f}{\partial\varepsilon}\right)\sigma(\varepsilon), \tag{5.7}$$

with f being the Fermi distribution function and

$$\sigma(\varepsilon)=\frac{e^2}{\pi\hbar}\sum_m\Lambda_m(\varepsilon). \tag{5.8}$$

The actual conductivity should be obtained by multiplication of factor four corresponding to the electron spin and the presence of K and K′ points. Note that eq. (2.16) of ref. 43 should be multiplied by two.

Figure 4 shows an example of the conductivity obtained by solving the Boltzmann equation. The Boltzmann equation

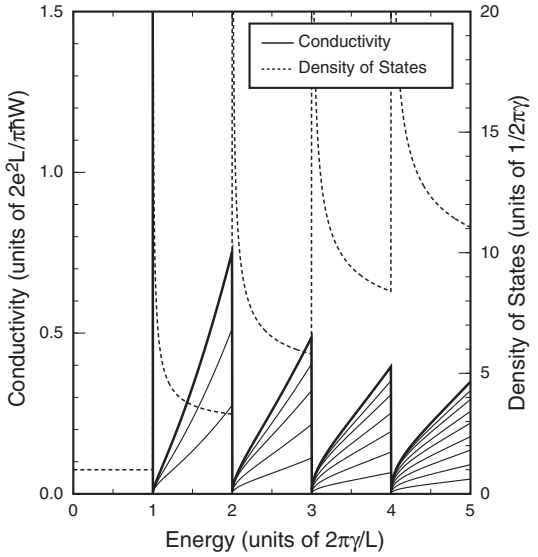

Fig. 4. An example of the energy dependence of the conductivity calculated using Boltzmann transport equation. The conductivity is infinite in the energy range $-1<\varepsilon L/2\pi\gamma<+1$ but becomes finite in the other region where there are several bands coexist at the Fermi level. The dashed line shows the density of states and thin solid lines show the contribution of each band to the conductivity (the lowest curve represents the contribution of $m=0$, the next two $m=\pm1,\ldots$).

gives an infinite conductivity as long as the Fermi level lies in the energy range $-1<\varepsilon L/2\pi\gamma<+1$ where only the linear metallic bands are present. However, the conductivity becomes finite when the Fermi energy moves away from this energy range into the range where other bands are present.

This conclusion is quite in contrast to the exact prediction discussed in the previous section that there is at least a channel which transmits with probability unity, leading to the conclusion that the conductance is given by $2e^2/\pi\hbar$ independent of the energy for sufficiently long nanotubes. The difference is highly likely to originate from the absence of phase coherence in the approach based on a transport equation. In fact, in the transport equation scattering from each impurity is treated as a completely independent event after which an electron looses its phase memory, while in the transmission approach the phase coherence is maintained throughout the system.

6. Effects of Inelastic Scattering

In order to take into account effects of inelastic scattering, we shall assume that the nanotube is separated into segments with length of the order of the phase coherence length and the electron looses the phase information after the transmission through each segment as illustrated in Fig. 5. The

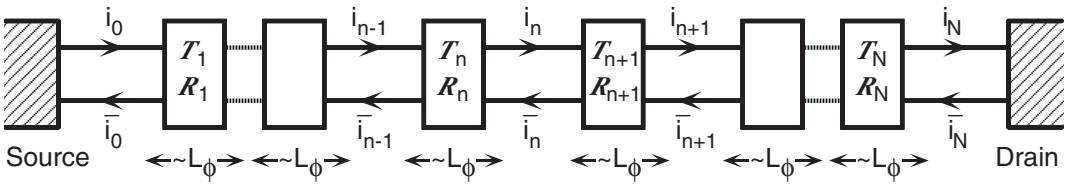

Fig. 5. A schematic illustration of separation of the nanotube into finite-length tubes determined by the phase coherence length L_ϕ. The length is chosen randomly so as to obey a Poisson distribution. The nanotube separated into N tubes is connected to the left and right reservoirs. Each tube is characterized by matrices $\mathcal{T}$ and $\mathcal{R}$ giving transmission and reflection probabilities among different in-coming and out-going channels.

transmission probability of the nth segment is described by $\mathcal{T}_n$ for modes incident from the left hand side and $\mathcal{T}_{\bar{n}}$ for modes incident from the right hand side. Similarly, the reflection probability of the nth segment is described by $\mathcal{R}_n$ for modes incident from the left hand side and $\mathcal{R}_{\bar{n}}$ for modes incident from the right hand side.

Explicitly, they are defined by

$$[\mathcal{T}_n]_{\beta\alpha} = |t^n_{\beta\alpha}|^2, \quad [\mathcal{T}_{\bar{n}}]_{\bar{\beta}\bar{\alpha}} = |t^n_{\bar{\beta}\bar{\alpha}}|^2,$$
$$[\mathcal{R}_n]_{\bar{\beta}\alpha} = |r^n_{\bar{\beta}\alpha}|^2, \quad [\mathcal{R}_{\bar{n}}]_{\beta\bar{\alpha}} = |r^n_{\beta\bar{\alpha}}|^2, \tag{6.1}$$

where t^n and r^n are transmission and reflection coefficients of the nth segment. When there are n_c right-going modes and n_c left-going modes, $\mathcal{T}$ and $\mathcal{R}$ are $n_c \times n_c$ matrices. In the present case with the time reversal symmetry we have $\mathcal{T}_{\bar{n}} = \mathcal{T}_n$ as has been discussed in §3.

The right- $\boldsymbol{i}_n$ and left-going current $\boldsymbol{i}_{\bar{n}}$ satisfy

$$\begin{aligned} \boldsymbol{i}_n &= \mathcal{T}_n \boldsymbol{i}_{n-1} + \mathcal{R}_{\bar{n}} \boldsymbol{i}_{\bar{n}}, \\ \boldsymbol{i}_{\bar{n}} &= \mathcal{T}_{\overline{n+1}} \boldsymbol{i}_{\overline{n+1}} + \mathcal{R}_{n+1} \boldsymbol{i}_n, \end{aligned} \tag{6.2}$$

where $\boldsymbol{i}_n$ and $\boldsymbol{i}_{\bar{n}}$ are n_c-component vectors consisting of the current associated with traveling modes. At the left reservoir, we have

$$\begin{aligned} \boldsymbol{i}_0 &= \boldsymbol{i}_{\mathrm{ext}}, \\ \boldsymbol{i}_{\bar{0}} &= \mathcal{T}_{\bar{1}} \boldsymbol{i}_{\bar{1}} + \mathcal{R}_1 \boldsymbol{i}_0, \end{aligned} \tag{6.3}$$

where $\boldsymbol{i}_{\mathrm{ext}}$ is the current determined by the left source reservoir and therefore same for all existing channels. At the right reservoir, we have

$$\begin{aligned} \boldsymbol{i}_N &= \mathcal{T}_N \boldsymbol{i}_{N-1}, \\ \boldsymbol{i}_{\bar{N}} &= 0, \end{aligned} \tag{6.4}$$

because there is no reflection at the reservoir.

This equation can be solved recursively. Define $\tilde{\mathcal{T}}_n$, $\tilde{\mathcal{T}}_{\bar{n}}$, $\tilde{\mathcal{R}}_n$, and $\tilde{\mathcal{R}}_{\bar{n}}$ to be the total transmission and reflection matrices for the segments $1, 2, \ldots, n$ combined. Then, when a segment $n+1$ is added, we have

$$\begin{aligned} \boldsymbol{i}_n &= \tilde{\mathcal{T}}_n \boldsymbol{i}_0 + \tilde{\mathcal{R}}_{\bar{n}} \boldsymbol{i}_{\bar{n}}, \\ \boldsymbol{i}_{\bar{n}} &= \mathcal{T}_{\overline{n+1}} \boldsymbol{i}_{\overline{n+1}} + \mathcal{R}_{n+1} \boldsymbol{i}_n, \end{aligned} \tag{6.5}$$

and

$$\begin{aligned} \boldsymbol{i}_{\bar{0}} &= \tilde{\mathcal{R}}_n \boldsymbol{i}_0 + \tilde{\mathcal{T}}_{\bar{n}} \boldsymbol{i}_{\bar{n}}, \\ \boldsymbol{i}_{n+1} &= \mathcal{T}_{n+1} \boldsymbol{i}_n + \mathcal{R}_{\overline{n+1}} \boldsymbol{i}_{\overline{n+1}}. \end{aligned} \tag{6.6}$$

Equation (6.5) is solved as

$$\begin{pmatrix} \boldsymbol{i}_n \\ \boldsymbol{i}_{\bar{n}} \end{pmatrix} = \begin{pmatrix} 1 & -\tilde{\mathcal{R}}_{\bar{n}} \\ -\mathcal{R}_{n+1} & 1 \end{pmatrix}^{-1} \begin{pmatrix} \tilde{\mathcal{T}}_n & 0 \\ 0 & \mathcal{T}_{\overline{n+1}} \end{pmatrix} \begin{pmatrix} \boldsymbol{i}_0 \\ \boldsymbol{i}_{\overline{n+1}} \end{pmatrix}. \tag{6.7}$$

Therefore, eq. (6.6) gives

$$\begin{pmatrix} \boldsymbol{i}_{\bar{0}} \\ \boldsymbol{i}_{n+1} \end{pmatrix} = \begin{pmatrix} \tilde{\mathcal{R}}_{n+1} & \tilde{\mathcal{T}}_{\overline{n+1}} \\ \tilde{\mathcal{T}}_{n+1} & \tilde{\mathcal{R}}_{\overline{n+1}} \end{pmatrix} \begin{pmatrix} \boldsymbol{i}_0 \\ \boldsymbol{i}_{\overline{n+1}} \end{pmatrix}, \tag{6.8}$$

with

$$\begin{pmatrix} \tilde{\mathcal{R}}_{n+1} & \tilde{\mathcal{T}}_{\overline{n+1}} \\ \tilde{\mathcal{T}}_{n+1} & \tilde{\mathcal{R}}_{\overline{n+1}} \end{pmatrix} = \begin{pmatrix} \tilde{\mathcal{R}}_n & 0 \\ 0 & \mathcal{R}_{\overline{n+1}} \end{pmatrix} + \begin{pmatrix} 0 & \mathcal{T}_{n+1} \\ \tilde{\mathcal{T}}_{\bar{n}} & 0 \end{pmatrix} \begin{pmatrix} 1 & -\tilde{\mathcal{R}}_{\bar{n}} \\ -\mathcal{R}_{n+1} & 1 \end{pmatrix}^{-1} \begin{pmatrix} \tilde{\mathcal{T}}_n & 0 \\ 0 & \mathcal{T}_{\overline{n+1}} \end{pmatrix}. \tag{6.9}$$

In terms of the transmission $\tilde{\mathcal{T}}_N$ of the whole segments combined, the conductance is given by

$$G = \frac{e^2}{2\pi\hbar} \tilde{\mathcal{T}}_N. \tag{6.10}$$

The actual conductance should be obtained by multiplication of factor four corresponding to the electron spin and the presence of K and K′ points.

In numerical calculations, the tube is divided into different segments with random length. The length of each segment is distributed according to the Poisson distribution

$$P(A) = \frac{A}{L_\phi^2} \exp\left(-\frac{A}{L_\phi}\right), \tag{6.11}$$

where L_ϕ is the inelastic scattering length. We have

$$\langle A \rangle = 2L_\phi, \quad \langle (A - \langle A \rangle)^2 \rangle^{1/2} = \sqrt{2} L_\phi. \tag{6.12}$$

Figure 6 shows some examples of calculated conductance for $W^{-1} = 100$ and $\varepsilon(2\pi\gamma/L)^{-1} = 1.5$ with $n_c = 3$. As long as the length is smaller than or comparable to the inelastic scattering length L_ϕ, the conductance is close to the ideal value $2e^2/\pi\hbar$ corresponding to the presence of a perfect channel. When the length becomes much larger than L_ϕ, the conductance decreases in proportion to the inverse of the length. When L_ϕ becomes comparable to the mean free path ($\Lambda_0/L \sim 6$ in the present case), the conductance becomes close to the Boltzmann result given by the dotted line.

In the present model, we have assumed that the phase coherence is maintained perfectly in each segment and is lost

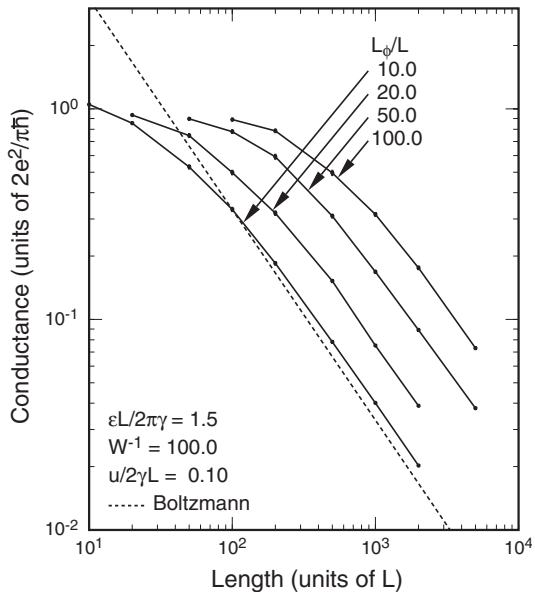

Fig. 6. An example of the conductance in the presence of inelastic scattering as a function of the length for different values of the phase coherence length L_ϕ.

suddenly after traversal over a segment. This is certainly a quite simplification of inelastic scattering effects and can become unrealistic when the phase coherence length becomes comparable to the mean free path. However, it is expected to be less unrealistic with the increase of the coherence length because phase-breaking scattering events occur less and less frequently. One possible way to take into account inelastic-scattering effects more properly is to attach many wires with current channels at random and connect them to a reservoir with a certain voltage[44] as has been made in quantum Hall systems.[45,46] Such calculations are very tedious and time consuming, and are left for a future study.

7. Summary and Conclusion

In summary, the presence of a single channel transmitting through the system without backscattering independent of energy has been proved in metallic carbon nanotubes for scatterers with potential range comparable to or larger than the lattice constant. Numerical calculations have shown that the conductance decreases from the ideal value determined by the number of traveling modes to that of a single mode with the increase of the length. The characteristic length is of the order of the mean free path obtained from a Boltzmann transport equation. Effects of inelastic scattering have been studied within a model that an electron looses its coherence for a distance determined by a phase coherence length. For a finite coherence length, the conductance decreases almost in proportion to the inverse of the length when the nanotube is sufficiently long. The conductance approaches that obtained by the transport equation with the decrease of the coherence length.

Acknowledgments

This work was supported in part by Grants-in-Aid for Scientific Research and for COE (12CE2004 ''Control of Electrons by Quantum Dot Structures and Its Application to Advanced Electronics'') from Ministry of Education, Culture, Sports, Science and Technology Japan. Numerical calculations were performed in part using the facilities of the Supercomputer Center, Institute for Solid State Physics, University of Tokyo.

1) S. Iijima: Nature (London) **354** (1991) 56.
2) N. Hamada, S. Sawada and A. Oshiyama: Phys. Rev. Lett. **68** (1992) 1579.
3) J. W. Mintmire, B. I. Dunlap and C. T. White: Phys. Rev. Lett. **68** (1992) 631.
4) R. Saito, M. Fujita, G. Dresselhaus and M. S. Dresselhaus: Phys. Rev. B **46** (1992) 1804; Appl. Phys. Lett. **60** (1992) 2204.
5) M. S. Dresselhaus, G. Dresselhaus and R. Saito: Phys. Rev. B **45** (1992) 6234.
6) R. A. Jishi, M. S. Dresselhaus and G. Dresselhaus: Phys. Rev. B **47** (1993) 16671.
7) K. Tanaka, K. Okahara, M. Okada and T. Yamabe: Chem. Phys. Lett. **191** (1992) 469.
8) Y. D. Gao and W. C. Herndon: Mol. Phys. **77** (1992) 585.
9) D. H. Robertson, D. W. Brenner and J. W. Mintmire: Phys. Rev. B **45** (1992) 12592.
10) C. T. White, D. C. Robertson and J. W. Mintmire: Phys. Rev. B **47** (1993) 5485.
11) H. Ajiki and T. Ando: J. Phys. Soc. Jpn. **62** (1993) 1255.
12) A. M. Rao, E. Richter, S. Bandow, B. Chase, P. C. EkIund, K. W. Williams, M. Menon, K. R. Subbaswamy, A. Thess, R. E. Smalley, G. Dresselhaus and M. S. Dresselhaus: Science **275** (1997) 187.
13) C. H. Olk and J. P. Heremans: J. Mater. Res. **9** (1994) 259.
14) J. W. Wildoer, L. C. Venema, A. G. Rinzler, R. E. Smalley and C. Dekker: Nature (London) **391** (1998) 59.
15) A. Hassanien, M. Tokumoto, Y. Kumazawa, H. Kataura, Y. Maniwa, S. Suzuki and Y. Achiba: Appl. Phys. Lett. **73** (1998) 3839.
16) T. Ando: Semicond. Sci. Technol. **15** (2000) R13.
17) T. Ando and T. Nakanishi: J. Phys. Soc. Jpn. **67** (1998) 1704.
18) T. Ando, T. Nakanishi and R. Saito: J. Phys. Soc. Jpn. **67** (1998) 2857.
19) T. Nakanishi and T. Ando: J. Phys. Soc. Jpn. **68** (1999) 561.
20) P. L. McEuen, M. Bockrath, D. H. Cobden, Y.-G. Yoon and S. G. Louie: Phys. Rev. Lett. **83** (1999) 5098.
21) A. Bachtold, M. S. Fuhrer, S. Plyasunov, M. Forero, E. H. Anderson, A. Zettl and P. L. McEuen: Phys. Rev. Lett. **84** (2000) 6082.
22) H. Ajiki and T. Ando: J. Phys. Soc. Jpn. **62** (1993) 2470 [Errata: **63** (1994) 4267].
23) H. Ajiki and T. Ando: Physica B **201** (1994) 349; *Proc. Int. Conf. Optical Properties of Nanostructures*, Jpn. J. Appl. Phys. **34** (1995) Suppl. 34-1, p. 107.
24) T. Ando: J. Phys. Soc. Jpn. **66** (1997) 1066.
25) N. A. Viet, H. Ajiki and T. Ando: J. Phys. Soc. Jpn. **63** (1994) 3036.
26) H. Suzuura and T. Ando: *Proc. 25th Inter. Conf. Phys. Semicond.*, ed. N. Miura and T. Ando (Springer, Berlin, 2001), p. 1525.
27) H. Ajiki and T. Ando: J. Phys. Soc. Jpn. **64** (1995) 260; *ibid.* **65** (1996) 2976.
28) H. Ajiki and T. Ando: J. Phys. Soc. Jpn. **64** (1995) 4382.
29) T. Ando: J. Phys. Soc. Jpn. **69** (2000) 1757.
30) T. Yaguchi and T. Ando: J. Phys. Soc. Jpn. **70** (2001) 3641; submitted to J. Phys. Soc. Jpn.
31) L. Chico, L. X. Benedict, S. G. Louie and M. L. Cohen: Phys. Rev. B **54** (1996) 2600.
32) M. Igami, T. Nakanishi and T. Ando: J. Phys. Soc. Jpn. **68** (1999) 716.
33) M. Igami, T. Nakanishi and T. Ando: J. Phys. Soc. Jpn. **68** (1999) 3146.
34) T. Ando, T. Nakanishi and M. Igami: J. Phys. Soc. Jpn. **68** (1999) 3994.
35) M. Igami, T. Nakanishi and T. Ando: J. Phys. Soc. Jpn. **70** (2001) 481.
36) H. J. Choi, J.-S. Ihm, S. G. Louie and M. L. Cohen: Phys. Rev. Lett. **84** (2000) 2971.
37) H. Suzuura and T. Ando: Physica E **6** (2000) 864; Mol. Cryst. Liq. Cryst. **340** (2000) 731; Phys. Rev. B **65** (2002) 235412.
38) J. C. Slonczewski and P. R. Weiss: Phys. Rev. **109** (1958) 272.
39) T. Ando and H. Tamura: Phys. Rev. B **46** (1992) 2332.
40) T. Ando: J. Phys. Soc. Jpn. **71** (2002) 2505.
41) T. Ando and T. Seri: J. Phys. Soc. Jpn. **66** (1997) 3558.
42) H. Akera and T. Ando: Phys. Rev. B **43** (1991) 11676.
43) T. Seri and T. Ando: J. Phys. Soc. Jpn. **66** (1997) 169.
44) M. Biittiker: Phys. Rev. B **32** (1985) 1846.
45) T. Ando: Surf. Sci. **361/362** (1996) 270.
46) T. Ando: Physica B **249–251** (1998) 84.